Modelling, Simulation and Validation of the Pneumatic End-Position Cylinder Cushioning

Fedor Nazarov, Jürgen Weber

Chait of Fluid-Mechatronic Systems, TU Dresden, Helmholtzstraße 7a, 01069 Dresden, Germany
E-mail: fedor.nazarov@tu-dresden.de (c/o), fluidtronik@mailbox.tu-dresden.de

Abstract

In this paper a model of the pneumatic cylinder with an integrated pneumatic end cushioning is presented. This model is needed to simulate and analyze the thermodynamical possesses in the pneumatic end cushioning and to elaborate a novel design strategy for damping systems with a higher capability on kinetic energy absorption and robust performance even with fluctuating operational conditions, such as supply pressure, inertial load or travel speed. To validate this model, the results of the experimentally based parametrization of the friction force in the cylinder sealings are compared for a Stribeck friction model and its modifications. A new approach suitable for an accurate approximation of the measured friction data within a wide range of pressure (2…8 bar_{rel}) and piston speed (0…0.8 m/s) is proposed. In the next step a flow rate characteristic of the integrated end cushioning throttle is experimentally obtained and analyzed. These data are used to parametrize the lumped parameters model of the cylinder with an end cushioning. Pressure and temperature in the cushioning volume and piston displacement are measured for different openings of the cushioning throttle to prove the validity of the model. The model will be used further for sensitivity analysis and robust optimization of the cushioning system design.

Keywords: pneumatic cylinder, end cushioning, thermocouple, friction, pneumatics, Stribeck curve, throttle

1 Introduction

Pneumatic drives find a widespread application in the modern industry. They are used as a cheap and reliable alternative to electric drives and as a front runner in some special industrial sectors. Pneumatic applications are essential in food, medical and diverse explosion-hazardous technologies, where they have gained a reputation of hygienic, safe, and reliable systems.

Within the last decades an integration of electronic control systems has made pneumatics smarter, safer, and simpler in both operation and design. However, time-costly manual works are still needed when setting up or adjusting some basic pneumatic components, as throttles or damping devises. Especially pneumatic end-position cylinder cushioning is very sensitive to any changes in operational conditions, setup and environment. Whenever one of those parameters has been changed, manual readjustment is usually needed. The latter has usually a trial-and-error nature. In parallel, a maximum quantity of energy, absorbed by the end-cushioning, often appears as a limitation factor when sizing the pneumatic cylinder designed to handle heavy objects. An engineer would rather prefer a larger-scaled cylinder with a proportionally higher damping capability to bring the moving mass softly and safely to the end position, even if a smaller cylinder is enough to perform the task. Large-scaling results directly in an increase in energy consumption whilst performing the same net work. For instance, the large-scaling is typical for nearly 80 % of all applications and avoiding the can contribute to reduction in energy consumption up to 40 % [1].

Having said that, the classical concept of pneumatic end-position cushioning needs to be investigated and revised to decrease its sensitivity against the operational conditions and enhance the energy absorption without enlarging the system or pushing up the costs. The first step towards this global goal is a development and validation of an accurate mathematical model of a pneumatic cylinder with a pneumatic end-position cushioning, which is discussed within this paper.

This accurate model is further needed to perform the sensitivity analysis and figure out the parameters with a highest impact on the damping capability of the end cushioning. These parameters, such as cushioning length, cushioning volume in a cylinder head, cushioning throttle conductivity as a function of the throttle opening, are accessible for the engineers on the design phase of a pneumatic cylinder. Hence, the global goal of the investigation of pneumatic end cushioning system is to find the optimal values of these design parameters corresponding to the maximum damping capability and simultaneously to guarantee a high robustness against the fluctuating operational environment, i. e. volatile supply pressure, alternating mass load or friction force.

This paper focuses only on the development, parameterization and validation of a simulation model of pneumatic cushioning device.

2 State of the art

In general, there are different ways to decelerate a moving mass within some limited stroke. The highest damping capability usually possess hydraulic shock absorbers that are also widely applied beyond pneumatic and hydraulic applications. They are reliable in operation and simple in modelling due to only a viscous term and spring force must be considered [2]. Hydraulic shock absorbers are very costly and need to be installed out of the cylinder. This increases the axial dimensions of the drive. A further approach of an external non-pneumatic cushioning is an elastic mechanical shock absorber. Such absorbers may have a good damping performance due to a sophisticated geometry and materials. That guaranties a constant deceleration within a short stroke [3]. However, mechanical dampers usually have a lower damping capability and durability when compared to hydraulic devices and can be applied only within a limited pressure range. External pneumatic damping devices that are free from the drawbacks of the integrated pneumatic cushioning are also present in the market, as for example [4]. As in case of the hydraulic shock absorbers they have high acquisition costs and need installation space out of the cylinder.

Having said that, is obvious, why the integrated pneumatic end cushioning is so widely used in the pneumatic cylinders. The main advantages are low costs, full integration into the cylinder head, reliability and ease of use. Several studies are devoted to the problematic of their simulation, adjustment and applicability. Wang et al. have developed a mathematical model of pneumatic end cushioning under assumption of an isentropic compression prosses in the end cushioning volume. The simulation of the piston speed, deceleration and pressure have shown good correlation with experiments. The inertial load was varied, and the other parameters were kept constant. The authors stated further potentials of model improvement with regards to consideration of the friction, fluid damping, leakage and discharge coefficients of pneumatic ports [5]. Beater has comprehensively studied the damping processes in the pneumatic cushioning as well. For this purpose, a Modelica-based simulation environment PneuLib was used. In this paper, damping capability as a function of the meter-out throttle and cushioning throttle conductance is studied. The author underlined a drawback of pneumatic cushioning in terms of its limited ability to absorb the kinetic energy at the end of the stroke. Especially crucial is a cylinder operation at a high speed. Besides this, the cushioning must be readjusted manually if the inertial mass is changed. The author also concludes a strategy for manual adjustment of the cushioning throttle [6].

Summing up, there are already some mathematical models of the pneumatic end cushioning existing, as well as some experimental studies are present. Nevertheless, none of them considers a thermal interrelation between the gas and the cylinder body in detail. Friction force model is also simplified or missing. In contrast, the present study aims for a more detailed consideration of the physical phenomena that may have a sufficient impact on the thermodynamical and mechanical parameters, relevant for the investigation and further optimization of the pneumatic cushioning system performance.

3 Mathematical model

Simulation of the physical processes, involved into deceleration of a cylinder piston, is essential for understanding the interrelations between the domains mechanics, tribology, fluid mechanics and thermodynamics. The mostly used approach for studying and designing pneumatic systems is a lumped parameter modelling, also known as a one-dimensional modelling. The simulation of one-dimensional models is commonly used to investigate the behavior of components, groups of components and complex pneumatic systems. This approach is used in this study as well. The model is implemented in the software SimulationX by ESI ITI GmbH. In the following paragraphs the implemented mathematical model of pneumatic cylinder is presented and discussed.

3.1 Force balance in a pneumatic cylinder

A typical example of a pneumatic cylinder with an integrated end cushioning is shown in the fig. 1. The functionality of the cushioning device is the same for the head and for the rod end. Due to a simpler geometry only the head end and therefore only the pull-in stroke is considered here. The speed of the piston (travel speed) is assumed to be controlled with a meter-out throttle, which is a very common industrial solution.

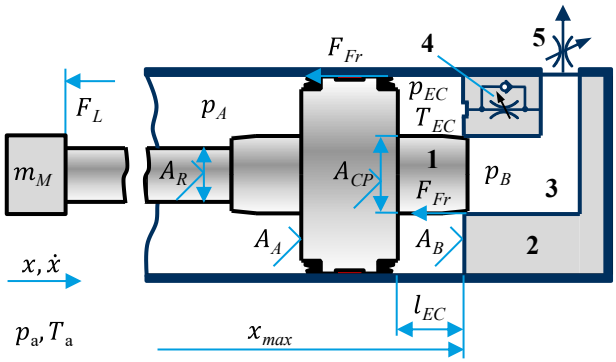

Figure 1: Simplified scheme of the pneumatic cushioning unit and its properties: 1 – cushioning plug, 2 – cylinder head, 3 – main outflow channel, 4 – end cushioning throttle (bypass channel), 5 – meter-out throttle.

The force balance is different for the main stroke ($l_{EC} < x < x_{max} - l_{EC}$), cushioning zone ($l_{EC} \geq x$ or $x \geq x_{max} - l_{EC}$) and the end position ($x = 0$ or $x = x_{max}$). For the main stroke eq. (1) applies:

$$m_M \cdot \ddot{x} = p_A \cdot A_A + p_a \cdot A_R - p_B \cdot A_B - F_L - sign(F_{Fr}) \tag{1}$$

Gravity force is not considered in eq. (1). If cylinder is mounted non-horizontally, the gravity force term can be considered implicitly as a part of for the load force F_L. After passing the main part of the stroke, cushioning plug overlaps the main outflow channel in the cylinder head. The air, constrained between the piston and cylinder head, shapes the cushioning volume with pressure p_{EC}, acting on the piston surface $A_B - A_{CP}$. The force balance for the cushioning region ($l_{EC} \geq x$ or $x \geq x_{max} - l_{EC}$) therefore differs from that for the main stroke:

$$m_M \cdot \ddot{x} = p_A \cdot A_A + p_a \cdot A_R - p_B \cdot A_{cp} - p_{EC} \cdot (A_B - A_{CP}) - F_L - sign(F_{Fr}) \tag{2}$$

In the end position ($l_{EC} = x = x_{max} - l_{EC}$) the resulting pressure force is balanced by so-called end force F_{end} acting on the cylinder head:

$$0 = p_A \cdot A_A + p_a \cdot A_R - p_B \cdot A_{cp} - p_{EC} \cdot (A_B - A_{CP}) - F_L - sign(F_{Fr}) - F_{end} \tag{3}$$

The value of the friction force in equations (1)-(3) can be defined using different approaches. Mostly used in pneumatic applications are dynamic LuGre and Dahl models [7, 8] and static Stribeck model [9, 10], polynomial speed-dependent function [11] and tangent function [2]. In this study the Stribeck model was used due to its simplicity and possibility to take into account the pressure and piston velocity dependence of the friction. According to [9] Stribeck friction model can be determined as:

$$F_{Fr} = F_{FC} + (F_{FS} - F_{FC}) \cdot e^{(-|\dot{x}|/v_S)} + k_v \cdot |\dot{x}|^a + k_p \cdot p_{AB-}. \tag{4}$$

Hereinafter differential pressure will be often mentioned in the text and therefore referred as a variable p_{AB-}:

$$p_{AB-} = |p_A - p_B| \tag{5}$$

Jianfeng applies a modified version of eq. (4) where F_{FC}, F_{FS} and k_v are linearly dependent on supply pressure and differential pressure in the cylinder chambers [12]. The function has three independent variables and 12 approximation coefficients and was verified by [13]. Depending on particular friction problem, available measured data and relevant range of operational pressures, speeds and forces, Stribeck model can be simplified, and the pressure-dependent term can be neglected [10, 14, 15]. For a wide variety of pneumatic applications, e. g. point-to-point tasks, the friction model can be reduced to a static and Coulomb friction forces or even assumed as a constant value, without significant decrease in the model quality. In such case parametrization turns out to be simple. Some cylinder producers provide values of static or Coulomb friction forces for their products. Alternatively friction can be evaluated with empirical studies.

For more elaborated problems, for example servo-pneumatic systems, where piston position and speed must be computed precisely, the eq. (4) cannot be further simplified and often advanced dynamic friction models, e. g. LuGre-model are applied.

3.1.1 Approximation of the friction force within the main piston stroke with a Stribeck function

For the studied problem of pneumatic end cushioning a friction model plays an important role for two reasons. Firstly, it impacts the dynamical behaviour of the piston according to eq. (1)-(3) and thus influences the quantity of kinetic energy that is absorbed by the cushioning device when decelerating the moving mass. Secondly, friction force, especially its viscous component, performs a dissipative work itself, that is it "helps" to decelerate the mass. All in all, the friction model for the stated problem must cover a wide variety of pressures and speeds that are peculiar for pneumatic applications. When talking about the relevant speed range, should be considered that over 90 % of all industrially applied cylinders have a stroke under 200 mm and thus have a short acceleration phase. Thus, they are unlikely to be operated at speed, sufficiently exceeding 1 m/s [16, 17]. With regards to the pressure, most of the pneumatic components are usually designed to operate at the maximum pressure of 10 bar_{rel}. In terms of energy efficiency, it also makes sense to decrease the supply pressure and use a larger cylinder, if high force is required [1]. Usually, pressure range up to 8 bar_{rel} and speed range up to 0.5 m/s are addressed in the literature [18].

The coefficients v_S, k_p, k_v and a in the eq. (4) are onerous to calculate analytically and keep under control during the experiment. They are impacted by such factors as cylinder temperature, properties of the sealing lubrication and sealing materials, sealing wear and quality of the frictional surfaces [19]. For this reason, these coefficients are usually determined experimentally to parametrize the friction function for the simulation model.

There are different concepts of test rigs for friction measurement existing. Many of them are comprehensively discussed in [17, 19]. For the given problem, a test rig according to the circuit in the fig. 2, A, was assembled. A cylinder Festo DSBF with diameter of Ø32 mm and stroke of 100 mm was studied. Pressure in cylinder chambers A and B, rod coordinate and acceleration were measured at various supply pressures $p_0 \in [2, \ldots, 8]$ bar_{rel} and 28 values of piston speed for each pressure. The horizontally moved mass amounted 3.7 kg. Additionally, pressure p_{EC} and temperature T_{EC} in the by-pass channel of the cushioning throttle were measured to obtain the friction force in the cushioning region and to have a reference for validation of the thermal part of the cylinder model respectively (fig. 2, B).

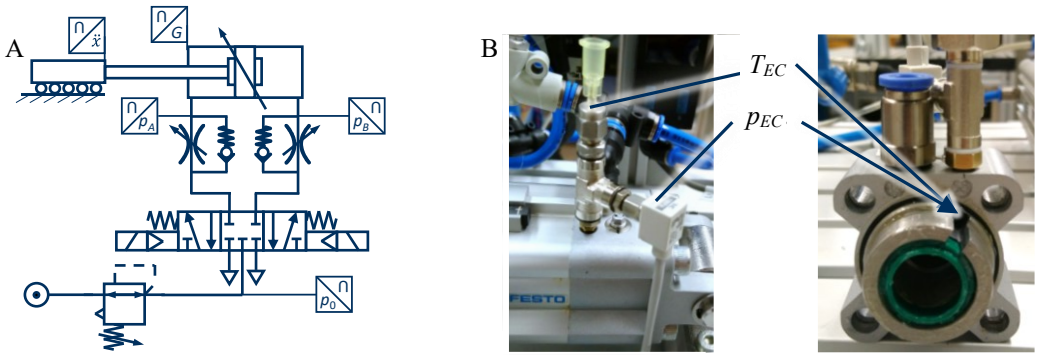

Figure 2: Circuit of the rig with tested cylinder with diameter of Ø32 mm and stroke of 100 mm (A, left) and adapter for the temperature and pressure sensors and their sensing point in the channel (B, right)

The maximum pressure was limited by 8 bar_{rel} due to the design of a directional valve (pressure limitation for internal supply of a pilot stage). Friction force of all friction pairs (i. e. piston and rod sealings and the rail housing) was estimated from eq. (1) on the part of the main stroke after reaching the quasistatic condition, i. e. constant travel speed, but before the piston enters a cushioning zone [19]. It must be noticed that the frictional phenomena and flow resistances between the pressure regulator and cylinder chambers result in a discrepancy of pressures p_A and p_B at various speed values. Besides, pressure drop between the p_0 and p_A sensing points is sufficient at high speed. Therefore, actual chamber pressures p_A and p_B must be used when fitting the model to the experimental data, and not the supply pressure p_0. Moreover, p_A and p_B fluctuate slightly even at the above-mentioned quasistatic condition. Figure 3 shows the effect of the pressure drop in the cylinder chamber when opening the meter-out throttle (i. e. setting the speed) as well as their variance for each speed value. Further in the study the median values of p_A and p_B were used to calculate the experimental friction force.

The experimental data were merged into a 28×7-matrix (number of throttle openings × supply pressures) and fitted to a Stribeck function (eq. (4)) with a nonlinear least square algorithm and plotted in the fig. 4, A, as a function of speed and pressure difference in cylinder chambers p_{AB}-. The obtained approximation coefficients are attached in Annex A.

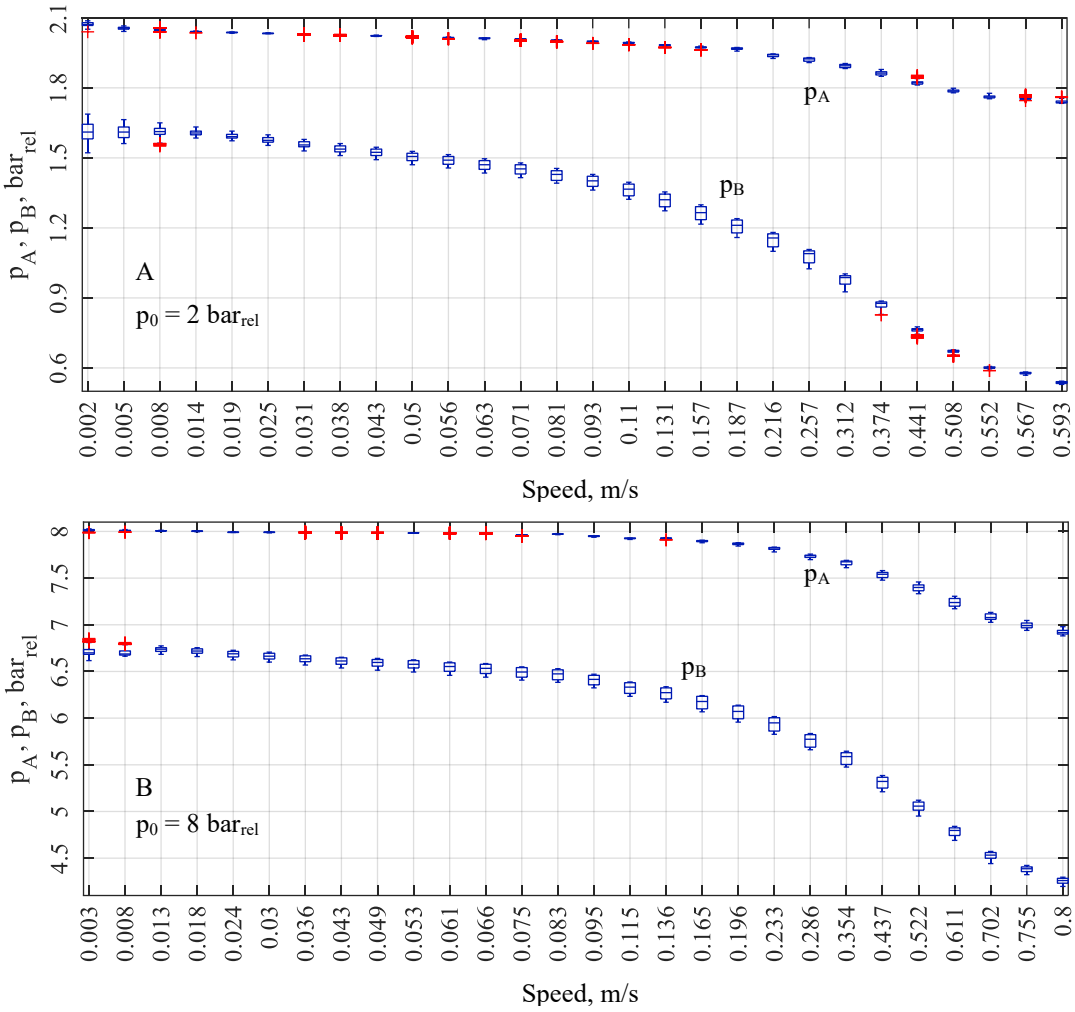

Figure 3: Variance of cylinder pressures p_A and p_B during the quasistatic part of the stroke depending on speed for supply pressure p_0 = 2 bar_{rel} (A, top) and p_0 = 8 bar_{rel} (B, bottom). Boxes correspond to the data between 25th and 75th percentile and are crossed by a median value. Outliers that are more than 1.5 times the interquartile range away from the body of the box are marked as "+".

It is obvious that eq. (4) has a constant gradient k_p along the pressure axis. The measured friction values tend to have a convex form along the pressure direction, whereas eq. (4) results in a stiff surface that does not cover the data, measured at a high pressure difference. Significant differences in the pressure slope by piston speed of 0.1, 0.3 and 0.5 m/s were also measured by [18] and [19]. The constancy of the pressure gradient k_p affects considerably the total performance of the approximation, measured as a residual sum of squared estimates of errors RSS and as a coefficient of determination R^2 (Annex A). The low-speed region is covered unsatisfactory as well. Stribeck speed v_S that determines a transition area between the dry and viscous friction, tends to be decreased by the nonlinear least-squares algorithm and meets the lower constraint at 0.001 m/s. The Coulomb friction is also restricted by the lower constraint at 2 N. Decreasing these bounds can result in a slightly better approximation performance but contradicts the engineering experience about the typical values of F_{FC} and v_S.

Further discussion of the eq. (4) leads to an unobviousness of the pressure difference $|p_A - p_B|$ in the last term. It implies that friction forces are equal when the piston is sliding with the same speed but different pressures p_A and p_B while the differential pressure is kept the same. For example, if in one case p_A = 7 bar and p_B = 5 bar, and in another case p_A = 3 bar and p_B = 1 bar, friction force would be the same at equal travel speed according to (4). However, the higher the pressure is, the tighter sealing lips are pressed to the frictional surfaces and the higher the frictional force is [19]. Hence, in the next step the pressure-dependent term in eq. (4) was modified to $k_p \cdot p_{AB+}$, where p_{AB+} is a summarized chamber pressure:

$$p_{AB+} = |p_A + p_B|. \tag{6}$$

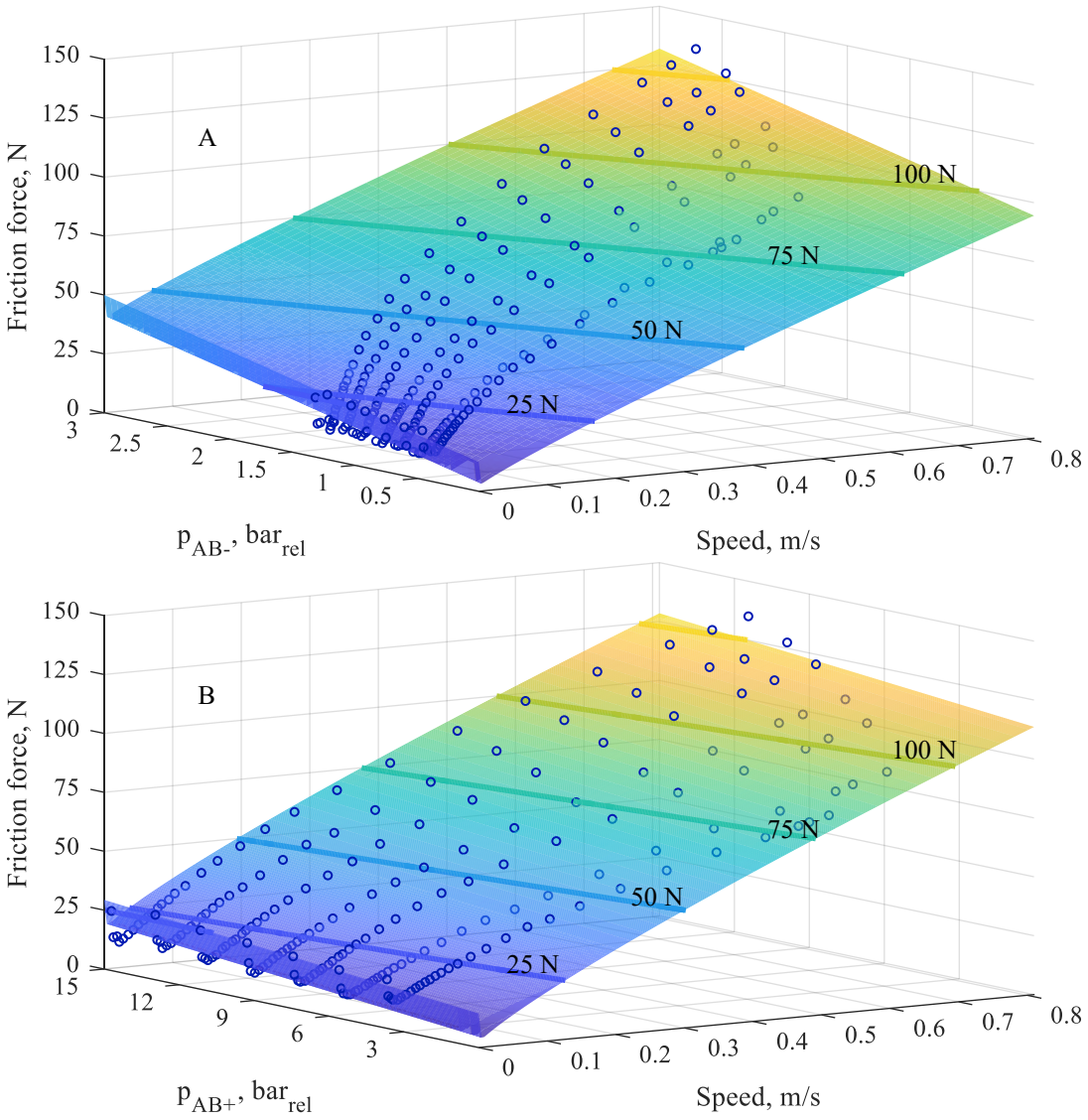

Figure 4: Experimental data (dots ○) fitted with approximation function (4) using differential p_{AB-} (A, top) and summarized p_{AB+} (B, bottom) pressures in the cylinder chambers.

Although the results of this substitution (fig. 4, B) may look slightly better in the low-speed area, the function is still linear in the pressure direction and cannot be applied for an accurate simulation of pneumatic end cushioning due to its low accuracy. The approximation coefficients for eq. (4) with $k_p \cdot p_{AB+}$ term are grouped in the Annex A.

3.1.2 Approximation of the friction force within the main piston stroke with a modified Stribeck function

To elaborate a handy and accurate function for a wide range of slide speeds and cylinder pressures, a simple approach is proposed here. In the first step, the measured data are fitted separately for each supply pressure p_0 with eq. (7). The real cylinder pressures p_A and p_B are not taken into account in this step.

$$F_{Fr} = b + (F_{FS} - F_{FC}) \cdot e^{(-|\dot{x}|/v_S)} + k_v \cdot |\dot{x}|^a \qquad (7)$$

In contrast to the eq. (4) a bias b appears in the first term instead of the Coulomb friction F_{FC}. Uncoupling the bias from the Coulomb friction significantly improves the quality of an approximation. The results are shown in the fig. 5 (pressure p_0 = 7 bar_{rel} is skipped). The estimated coefficients and approximation performance are attached in the Annex B.

It is noticeable that the form of the curves in the viscous region ($\dot{x} \gg v_S$) may be not convex as in the given case, but also concave for some larger cylinders, as for example, the cylinders with diameters of Ø40, Ø50 and Ø80 mm measured by [18]. Basically, this form depends on the sealing material, their form, the rheological properties of the lubrication and the testing methodology [19]. All in all, the eq. (7) approximates the measurements very accurately.

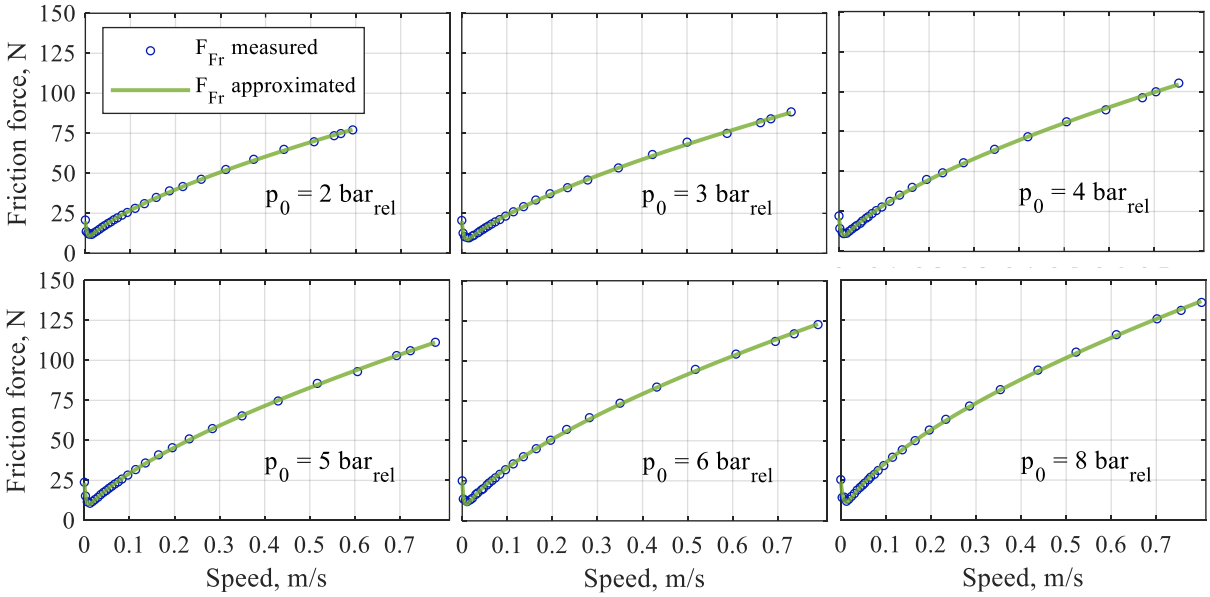

Figure 5: Friction force for supply pressure $p_0 \in [2,3,4,5,6,8]$ bar_{rel}.

In the second step, the correlation between the coefficients b, F_{FS}, F_{FC}, v_S, k_v, a and supply pressure p_0 must be analysed. For v_S, F_{FC} and a no obvious correlation can be derived, whereas for the other coefficients a descending or ascending trend is observed with an increase of p_0. It is important to repeat that chamber pressures p_A with p_B and not p_0 are relevant for the real frictional behaviour of the cylinder. However, at high slide speed and constant p_0, chamber pressures vary noticeably, as was shown in the fig. 3. Nevertheless, p_A and p_B do correlate with p_0. An increase of p_0 results inevitable in an increase of p_A and p_B. Thus, p_0 can be treated as a variable that correlates implicitly with the friction force, provided that the test circuit and is not changed and no new forces appear in the system.

Considering this, the pressure-dependent coefficients b, F_{FS}, and k_v are linearised with a function $i_0 + p \cdot i_1$, where i corresponds to each of these three coefficients and p is some pressure value, used to estimate the friction. In the following, differential pressure p_{AB-} and summarized pressures p_{AB+} are used as this pressure value in the friction function. Here again, p_0 should not be applied as a variable p, because it does not reflect any changes in the external load force F_L or inertial force $m_M \cdot \ddot{x}$ (see eq. (1)) that affect p_A and p_B and thus real pressure-dependent frictional forces. In the given case, load force and inertial mass remained constant during the friction measurements, but they will be varied in the further steps and thus p_0 is not considered for friction calculation. Applying the pressure-linearized coefficients to eq. (7) following two-dimensional function is obtained:

$$F_{Fr} = b_0 + b_1 \cdot p_{AB-} + (F_{FS.0} + F_{FS.1} \cdot p_{AB-} - F_{FC}) \cdot e^{(-|\dot{x}|/v_S)} + (k_{v.0} + k_{v.1} \cdot p_{AB-}) \cdot |\dot{x}|^a \qquad (8)$$

The results of approximation with eq. (8) are plotted in the fig. 6, A. Figure 6, B, corresponds to the same function, but with p_{AB+} applied instead of p_{AB-}. Both versions perform greatly in the whole range of pressures and piston speeds with coefficients of determination R^2 of 0.9975 and 0.9969 respectively (see Annex C).

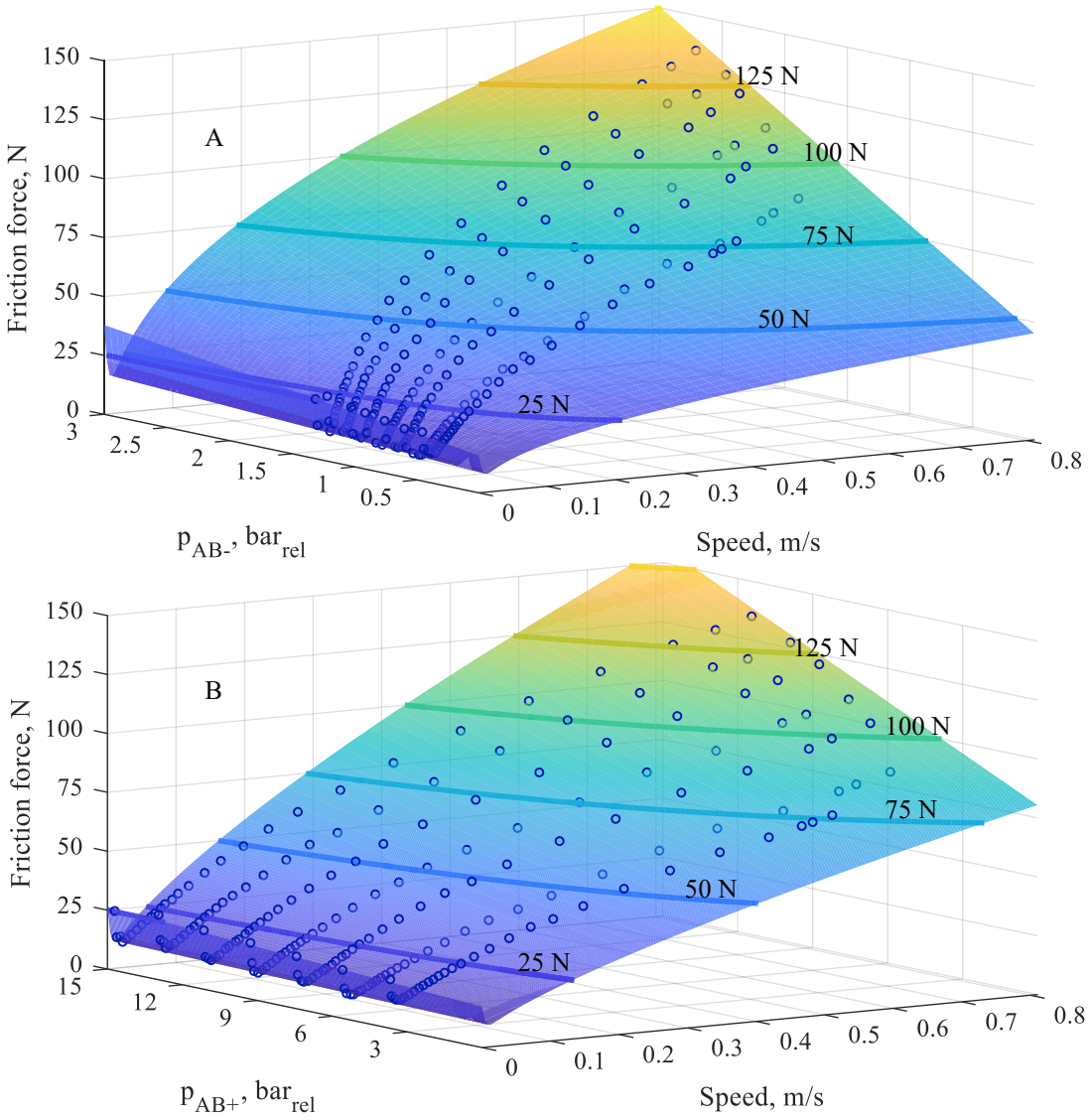

Figure 6: Experimental data (dots ○) fitted with approximation function (8) using differential p_{AB-} (A, top) and summarized p_{AB+} (B, bottom) pressures in the cylinder chambers.

One of the advantages of the proposed method and function (8) is that the terms $i_0 + p \cdot i_1$ preserve their physical meaning. This is handy when seeking out an error or setting the constraints and initial values for the least-square algorithm. In the following study the model with summarized pressures p_{AB+} is used.

3.1.3 Approximation of the friction force in the end cushioning zone with a modified Stribeck function

For the end cushioning region friction force must be obtained separately. Friction force in the end cushioning differs from the friction within the main stroke because of the additional tribological pair between the damping plug and the damping sealing as shown in the fig. 1. When the cushioning length is reached, cylinder piston starts to decelerate, and its speed is not constant anymore. Therefore, to derive the *p-v*-dependence of the friction there, speed values as differentials *dx/dt* between each neighbour points were divided into some groups, which are defined by speed levels. All the calculated speed values that are laying between some two following levels are asserted to the group. Then, the speed values and friction forces, calculated for them from eq. (2) using the measured pressure in the cushioning volume p_{EC}, are statistically evaluated to estimate the median value of the friction and its variation for each speed group. An example for 13 levels and 12 groups of speed at $p_0 = 4$ bar_{rel} is shown in the fig. 7, A. On the boxplot each speed group corresponds to the mean value of its levels. As to be seen, the median values of the friction force tend to form some kind of Stribeck curve. For this reason, all the points measured in the end cushioning region were fitted with eq. (8) for various pressures p_{EC} in the cushioning volume. The results are plotted in the fig. 7, B, and the estimated coefficients are attached in the Annex C.

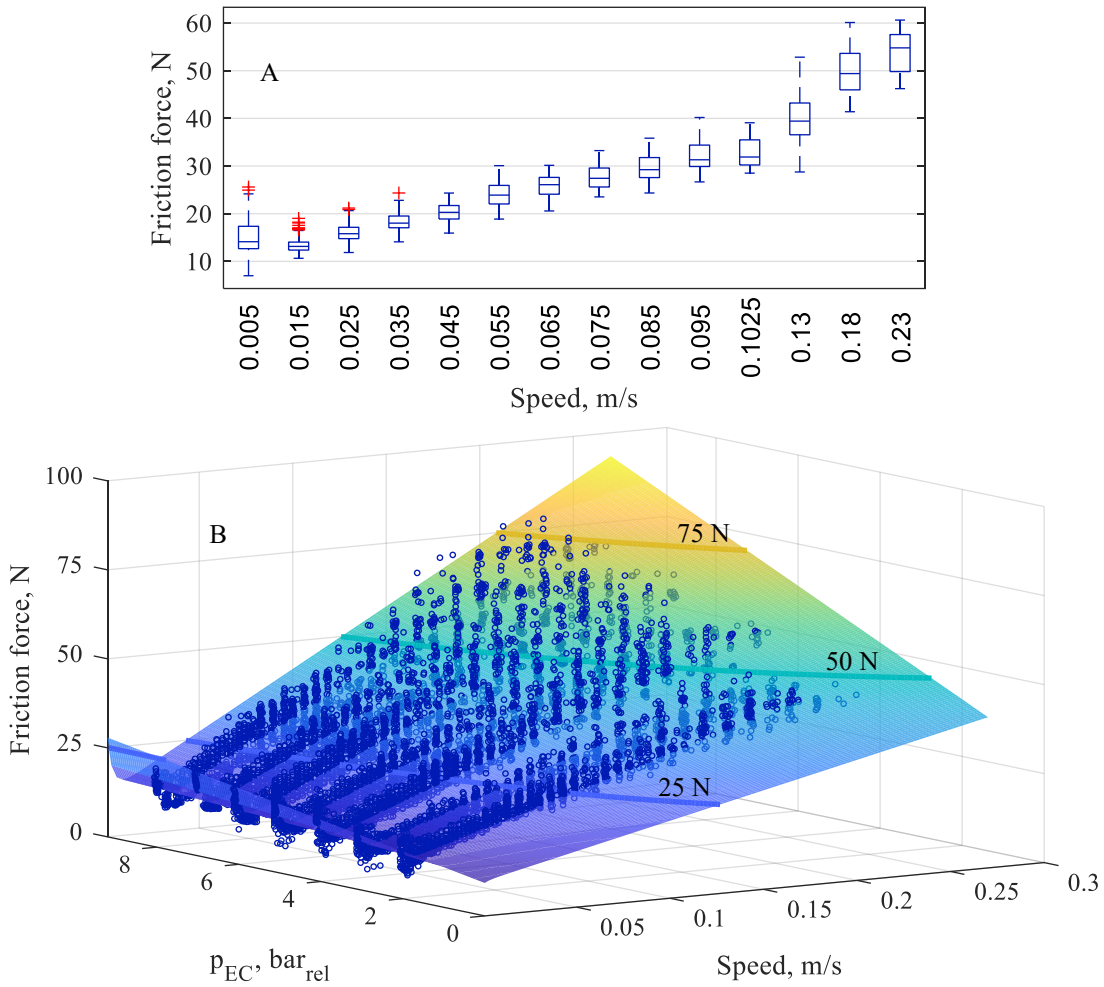

Figure 7: Measured friction forces for 12 groups of speed values in the cushioning zone at supply pressure p_0 = 4 bar_{rel} (A, top) and approximation of the friction in the end cushioning with eq. (8) (B, bottom).

Summing up the results of this paragraph, the proposed mechanical model is used for simulation of the piston movement subject to the presence of the end cushioning. The piston coordinate appears as a switch between the values of the coefficients for the main stroke and for the end cushioning zone. It is important to use separate models for the main stroke and for the end cushioning zone because of the different pressure forces acting on the piston and the different tribological pairs due to the presence of the end cushioning sealing.

3.2 Thermodynamic model of the air flow

To model the air flow and the transient pressure changes, following equations (9)-(12) for a one-dimensional control volume are numerically solved in the simulation environment. Variables with the low-case "1" correspond to the inlet parameters of the volume, with low-case "2" to the outlet, and without index to the volume itself.

As mentioned before, most pneumatic applications are limited by pressure of 10 bar_{rel}, in some rare cases of 16...20 bar_{rel}. Air temperature in pneumatic systems may oscillate in a range of ±20…60 °C around the ambient conditions, and usually for a very short time, i. e. for few milliseconds or seconds. Within this temperature and pressure range, a dry compressed air may be treated as an ideal gas because of only a slight variation of specific heats (less than 3.5 % for c_p and less than 1 % for c_V) [20]. When talking about the applications of a high-pressure-pneumatics, or systems exposed to extreme temperature amplitudes, this simplification may result in a high error. However, when talking about the vast majority of industrial pneumatic systems, ideal gas law is applicable:

$$p \cdot V = m \cdot R \cdot T \tag{9}$$

Conservation of momentum:

$$\Sigma F = \frac{d}{dt}(\rho \cdot v \cdot V) + \dot{m}_2 \cdot v_2 - \dot{m}_1 \cdot v_1 \tag{10}$$

Conservation of mass:

$$\dot{m}_1 = \rho_1 \cdot v_1 \cdot A_1 = \frac{d}{dt}(\rho \cdot V) + \rho_2 \cdot v_2 \cdot A_2 \tag{11}$$

Conservation of energy with neglected leakages and potential energy of the air:

$$\dot{Q} + \dot{W} = \dot{U} + \dot{m}_2 \cdot \left(h_2 + \frac{{v_2}^2}{2}\right) - \dot{m}_1 \cdot \left(h_1 + \frac{{v_1}^2}{2}\right) \tag{12}$$

Heat transfer equation:

$$\dot{Q} = \alpha \cdot A \cdot (T_W - T) \tag{13}$$

From the eq. (9)-(13) equations for the transient pressure and temperature changes in the considered volume can be derived [2]. Another important relation concluded from the (9) and (12) is an isentropic flow rate equation:

$$\dot{m} = A_2 \cdot \sqrt{2 \cdot p \cdot \rho} \cdot \sqrt{\frac{\kappa}{\kappa - 1} \cdot \left[\left(\frac{p_2}{p}\right)^{2/\kappa} - \left(\frac{p_2}{p}\right)^{(\kappa+1)/\kappa}\right]} \tag{14}$$

It can be approximated with an elliptic function (15), which is widely used in pneumatics to calculate subsonic mass flow rate streaming out of the volume with constant pressure p through a pneumatic resistance with back-pressure p_2. When the air flow reaches the sonic speed in the smallest cross-section of the resistance, the mass flow rate remains constant (chocked) even if p_2 is reduced further. For this part of the flow diagram eq. (16) applies [21]:

$$\dot{m} = C \cdot \rho_a \cdot p \cdot \sqrt{\frac{T_a}{T_1}} \cdot \sqrt{1 - \left(\frac{p_2/p - b}{1 - b}\right)^2} \qquad for\ \frac{p_2}{p} \geq b \tag{15}$$

$$\dot{m} = C \cdot \rho_a \cdot p \cdot \sqrt{\frac{T_a}{T_1}} \qquad for\ \frac{p_2}{p} \leq b \tag{16}$$

Air density ρ_a and temperature T_a correspond to the atmospheric conditions according to the ISO 6358.

3.2.1 Parametrization of the meter-out throttle

Sonic conductance C and critical back-pressure ratio b from eq. (15)-(16) are properties of some particular pneumatic resistance. Usually, they are given explicitly or implicitly (i. e. can be derived from the flow diagrams) in the datasheets of throttles and valves. They also can be estimated experimentally on a test rig with standardized dimensions as stated in the ISO 6358. Because the meter-out and end-cushioning throttles are settled manually it is worth to assess the value of the random error caused by inaccurate throttle adjustment. In the fig. 8 a polynomial approximation of the meter-out throttle sonic conductance C_{MO} is plotted versus the number of the knob revolutions z_{MO}. The experiment was repeated 8 times, the inlet pressure was kept constant at p = 7 bar_{abs}.

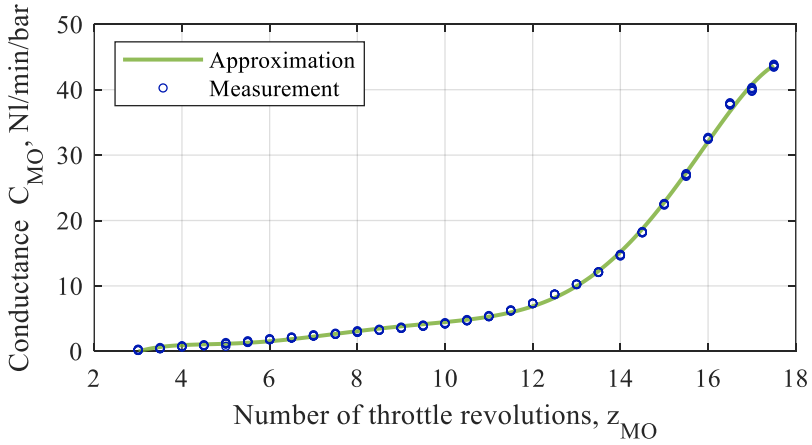

Figure 8: Sonic conductance of the meter-out throttle as a function of the number of throttle revolutions: 8 measurements and their polynomial approximation.

Generally, the absolute difference between the measured median conductance and its approximation is very low. But at small openings (under 6 revolutions) approximation error and random error can cause considerable relative error. This results in speed deviation between experiment and simulation. However, the low-speed range at $z_{MO} < 6$, which corresponds to ca. 2.5 cm/s at $p_0 = 8$ bar_{rel}, is less relevant for the end cushioning problem because kinetic energy is proportional to the speed squared. In this context more important is an impact of the deviations in C_{MO} at a higher opening range over 16 revolutions.

Applying the estimated characteristic $C_{MO}(z_{MO})$ and critical pressure ratio of $b_{MO} = 0.45$ (measured for a fully opened throttle with two 90°-angle pneumatic fittings) to equations (15)-(16) the mass flow rate through the throttle can be calculated. The pressure p before the throttle is estimated from the force balance equations (1)-(8) and the back-pressure p_2 depends on the conductance of the pneumatic hose and the directional valve. For the simulation of pneumatic hoses, the model by Bala validated by Hepke was used [9, 22]. The directional valve can be considered using the same *C*-*b*-model. This step as well as the parametrization of the circuit segment "air source → cylinder chamber A" is analogous and therefore skipped here.

3.2.2 Investigation and parametrization of the end cushioning throttle

In the contrary to throttles, directional and servo-valves, the data about the conductance of the end cushioning throttles are not given in any of the catalogues known to the authors. By this reason the flow characteristic of the end cushioning throttle was measured experimentally in this study. For this measurement the piston of the tested cylinder was fixed at the position $x = x_{max} - l_{ec} - 4$ mm. In this position the cushioning volume V_{EC} is connected with the cylinder outflow channel only through the end cushioning throttle. The air supply to the V_{EC} was carried out through the bore in the cylinder wall at the coordinate $x = x_{max} - l_{ec}/2$ (half the cushioning length from the cylinder head). The static pressure $p = p_{EC}$ in the cushioning volume was controlled with a sensor through another bore and kept constant at 7 bar_{abs}. The air temperature before the studied throttle was controlled with a thermocouple shown in the fig. 2, B. Back-pressure p_2 was adjusted with another throttle and measured in the outlet of the cylinder head. Figure 9 shows the measured and approximated characteristic $C_{EC}(z_{EC})$ and the flow rate characteristics for $C_{EC} = 24$, 16 and 8 Nl/min/bar.

The approximated conductance function (fig. 9, A) slightly deviates from the measurements at throttle openings under 1.5 rev. The curvature is characterized with three different gradients: low gradient within the first 1.5 rev., high gradient between 1.5 and 3.5 rev. and a less sloping part above 3.5 rev. The use of a low and high conductance gradients is convenient to enable the fine throttle adjustment for low and high piston speeds.

A particular feature of the measured flow rate diagram in the fig. 9, B, is a high value of the critical ratio *b* at the full opening. For two-atomic gases and above-mentioned pressure and temperature boundaries of pneumatic applications this value is limited by $b = 0.528$, if the pneumatic resistance is treated closely to an ideal nozzle. However, the geometry of the cushioning throttle differs from that of the ideal nozzle. In the most pneumatic cylinders, the cushioning throttle is implemented as a needle throttle, and not as a common throttle with an axial gap. At a small opening the length of the gap in the needle throttle is sufficient compared to its height [20]. Therefore, the friction losses along this gap length are not negligible anymore, and the equation (14) cannot be derived from the energy conservation (12) in this case. Regardless of that fact, according to ISO 6358-1:2013 the equations (15) and (16) are applied as approximation functions to characterize various pneumatic components with non-negligible friction losses, such as pneumatic tubes, that may also have high critical ratio *b*.

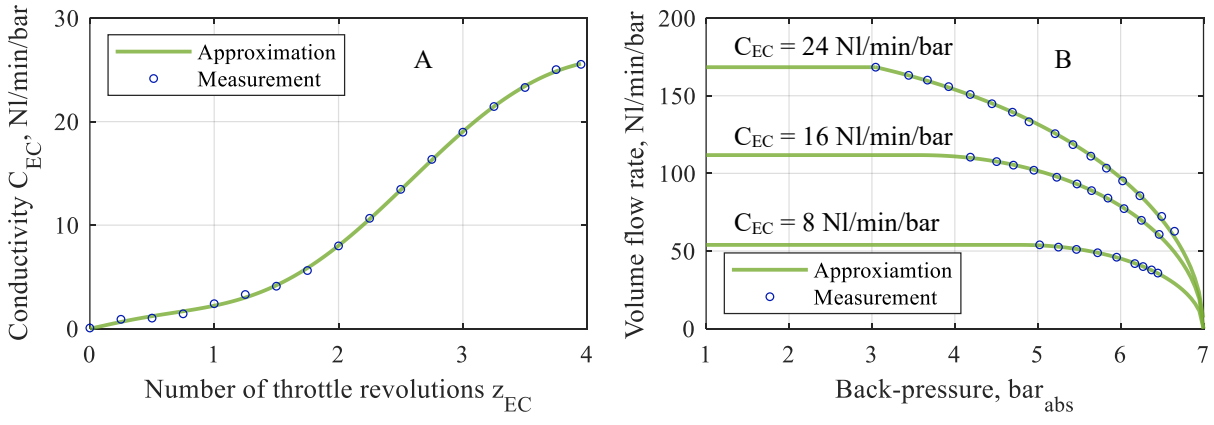

Figure 9: Measured and approximated conductance characteristic $C_{EC}(z_{EC})$ (left, A) and the flow rate characteristics *for different openings of the end cushioning throttle at constant inlet pressure $p_{EC} = 7$ bar_{abs}.*

In case of the studied end cushioning throttle, parameter b_{EC} was specified in the model as a linear function of the pneumatic conductance C_{EC}. As discussed above for the meter-out throttle, the approximated measured data for $C_{EC}(z_{EC})$ and $\dot{m}(p_2/p_{EC})$ describe an interrelation between the pressure in the cushioning volume and the mass flow rate through the cushioning throttle and hence the speed of the piston in cushioning region.

3.3 Heat transfer model

Heat transfer between the compressed air, cylinder wall and environment is not negligible in pneumatic systems and must be considered to achieve the results comparable with reality. Temperature changes in a pneumatic cylinder are usually caused by pressurizing or discharging the cylinder chambers. For instance, Hassan et al. has measured the temperature fluctuations between 0 and 60 °C in a Ø50 mm cylinder with a stroke of 200 mm [23]. Hepke has compared experimentally the temperature response of three air reservoirs made of polyvinylchloride (PVC), aluminium alloy and stainless steel when charging them from 1 to 7 bar_{abs}. He figured out that the temperature rises in the PVC-reservoir up to 120 °C and drops down within several seconds. In case of aluminium and steel, which are more relevant materials for pneumatic cylinders and reservoirs, the temperature increases up to 55 and 75 °C respectively. Carneiro and Almeida have proposed a new method for the calculation of the heat transfer coefficient based on the measurements of the pressure response when charging different cylinders [24]. The authors concluded that the cylinder material, whether it is a stainless steel or an aluminium alloy, is not relevant for modelling of the thermal processes in such an extent as the inner cylinder geometry, i. e. the area exposed to the heat transfer, is. Further, De Giorgi et al. proposes an accurate method for comprehensive modelling of the thermal domain in pneumatic systems and underline an inapplicability of often used polytropic, adiabatic, or isothermal models for accurate calculations [25].

Consideration of thermal interrelations in pneumatic cylinder is very important when talking about the calculation of energy consumption. Usually, energy consumption is calculated for cylinder as an isothermal system, and gas temperature in the chambers is assumed to be equal to the environmental temperature. However, when a cylinder with a small stroke is operated at a high frequency, the air may not cool down completely and fills the cylinder chamber at higher temperature and thus at a lower density at the same pressure. This results in a lower air consumption compared to an isothermal system. In terms of pneumatic end cushioning, an ability of a cylinder body to carry the heat away during the damping phase has an impact on a total energy absorption capability of the cushioning system.

To estimate the heat transfer coefficients in a one-dimensional model of pneumatic cylinder, the approach used by Michel for modelling the thermal behaviour of compact electrohydraulic drives [26] was transferred to the pneumatic systems. According to this approach, a cylinder body can be decomposed into heat capacities with a simple geometry, such as the cylinders, rods or plates, which are streamed with an air flow longitudinally or orthogonally. These capacities are connected with each other and with pneumatic part of the model via thermal resistances, each characterized by heat conductance or heat transfer coefficient for free or forced convection. For simple geometries heat transfer coefficients can be easily estimated with low computation costs.

4 Results and discussions

To validate the simulation model of pneumatic end cushioning, static pressure p_{EC} and temperature T_{EC} in the cushioning volume as well as cylinder rod coordinate were measured. The sensing point for both temperature and pressure is shown in the fig. 2, B. For temperature measurements a thin K-type thermocouple Omega CHAL-0005 was used. It has a bare sensor head, and with diameter of 12.5 µm its cross-sectional area is about 25 times smaller than that of a human's hair. Low thickness results in a low heat capacity of the sensor head and consequently in a short response time. Unfortunately, no exact data about the response time of this model can be obtained from the datasheets. Besides, the heat transfer from the gas to a sensor head via convection depends on air density and flow speed. Thus, the time constant may be defined only for one operational point, whereas the measured air parameters in the cushioning channel vary significantly. To estimate at least a rough value of the time constant, the sensor head was exposed to a temperature change with an amplitude of 40 °C within under 2 ms at upstream velocity of 5 m/s. From the exponential response plots the time constant of about 15 ms was determined. That means, the sensors head is expected to take the temperature of the air within about 75 ms. The reaction time of the signal amplifier of 0.5 ms is therefore negligibly small when considering the entire measuring circuit. Using this time constant in the model, a signal from the thermocouple can be simulated as a PT1-element and its output is expected to be comparable with the measured temperature. The data were acquired with an oscilloscope. Time constant of the sensor Omega 5TC-TT-KI-40-1M used by [9] with diameter of Ø75 µm was measured by 90 ms and thus has reaction time of ca. 450 ms. Sensors used by [23] have the same diameter and thus are expected to have the similar dynamic properties.

A significant drawback of the Ø12.5-µm-thermocouples is their fragility. The thermocouples were glued into a G20 syringe needle, and the needle was sealed with an industrial feedthrough. For pressure measurement small sensor SMC PSE540 with response time of 1 ms and M3-connection was used. The aim was to minimize the infliction of an additional dead volume brought about by the sensors, bore in the cylinder head and an adapter. The results of the measurements for supply pressures p_0 = 5 bar_{abs} and p_0 = 7 bar_{abs} for 16 meter-out throttle revolutions (almost full throttle opening) and three openings z_{EC} of the end-cushioning throttle are shown in the fig. 10-11.

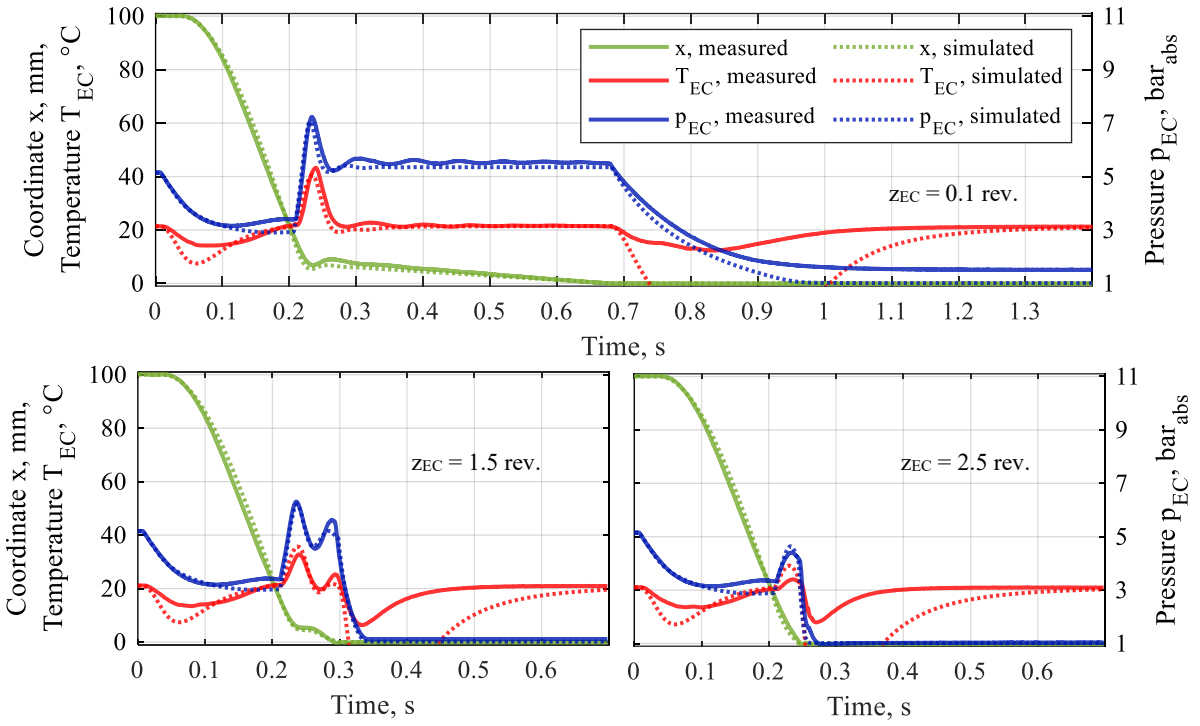

Figure 10: Piston stroke x (green), cushioning temperature T_{EC} (red) and pressure p_{EC} (blue) measured for different openings of the end cushioning throttle at p_0 = 5 bar_{abs} and moving mass m_M = 3.7 kg.

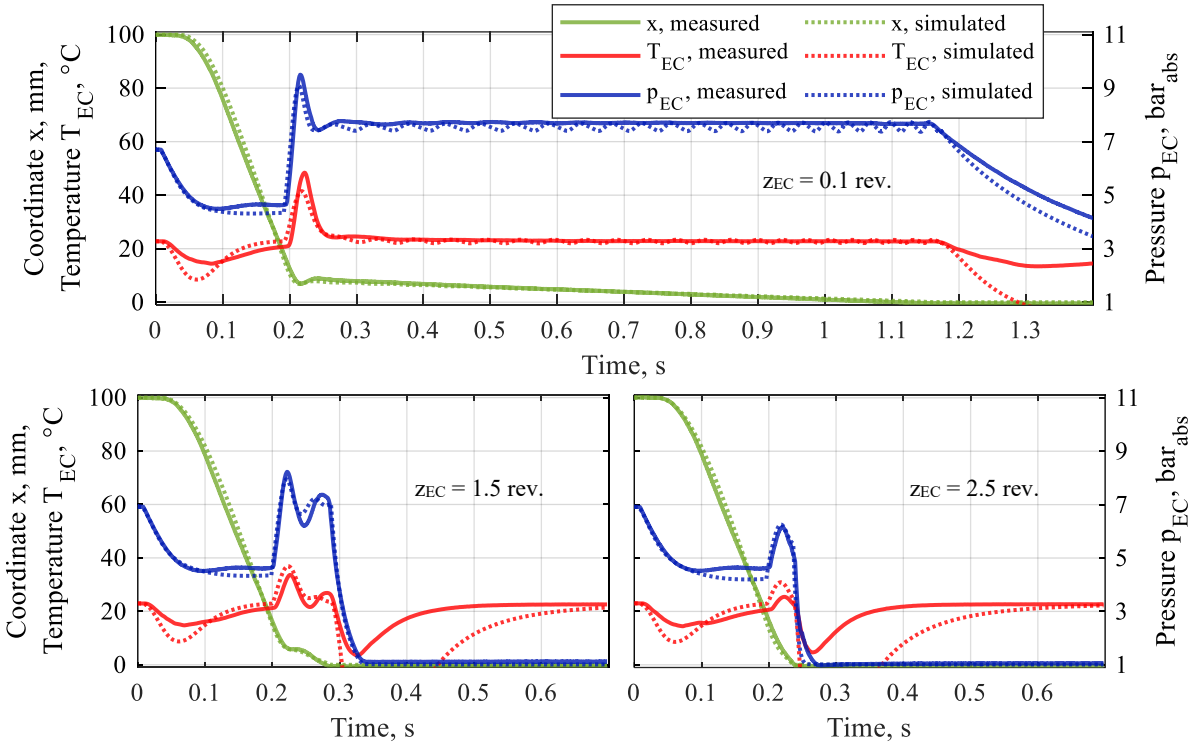

Figure 11: Piston stroke x (green), cushioning temperature T_{EC} (red) and pressure p_{EC} (blue) measured for different openings of the end cushioning throttle at p_0 = 7 bar_{abs} and moving mass m_M = 3.7 kg.

Each of the three subplots in the fig. 10-11 depicts distinctive cushioning possesses that typically occur in industrial applications. At very small cushioning throttle opening $z_{EC} = 0.1$ rev. (top subplots), the pressure rises significantly as soon as the cushioning region is reached by the piston. The piston springs back, but without touching the cylinder head. Because the most part of its kinetic energy is already absorbed and the throttle conductance is very low, the piston travels to the end position slowly. This is an example of a cushioning process with an overdamping. If there is no strict limitation on travel time, this setting is rather harmless because no shock, noise or vibration occur. It is worth mentioning that an increase of the moving mass above 10 kg leads to a situation, when inertia pushes the piston through the damping volume, and it reaches the cylinder head in the first oscillation phase whilst not being completely decelerated. That means that kinetic energy exceeds the maximum damping capability of the integrated cushioning for a given cylinder because no further closing of the cushioning throttle is possible. Either mass or speed must be reduced.

Another important issue must be noted, when comparing travel time in both top subplots of the fig. 10-11. In both cases the cushioning throttle was adjusted manually and was supposed to be the same. However, even a small error in the manual adjustment results in considerably different travel time. In one case the piston passes the cushioning zone within 0.48 s, in another case within this time doubled. This phenomenon illustrates well the sensitivity of the pneumatic end cushioning on the manual adjustment.

Discussing the plots for further throttle openings, is important to emphasize that in the most pneumatic applications travel time plays a major role and must be reduced to a minimum to enhance the output machine productiveness. Having said that, an optimal adjustment of the cushioning throttle is usually sought to keep the cushioning time as short as possible. A relative example is shown in the left subplots of the fig. 10-11 for cushioning throttle opening $z_{EC} = 1.5$ rev. Damping pressure increases not as significant as in the first case, piston does not rebound, but the pressure is sufficient to slow down the mass before it reaches the end position. A small amount of the rest energy may be buffered by an elastic shock absorber installed in the cylinder. No harmful vibration appears, but a quiet, soft knock may be heard. Travel time in the cushioning zone decreases to 0.08…0.09 s. Further opening of the cushioning throttle, e. g. up to 2 revolutions leads to an increase of the piston speed at the very last part of the stroke of ca. 5-8 mm: being once decelerated, piston accelerates again and hits the cylinder head. Stacking the mass up to total maximum of 10 kg is not crucial at $z_{EC} = 1.5$ revolutions and only changes the form of the stroke-time-profile closer to a monotonous sine-like deceleration.

The example of an underdamped cushioning setting is shown in the right subplots of the fig. 10-11. The conductance of the throttle is so high that the air flow out of the cushioning volume meets almost no resistance and no braking pressure is built up. As a result, piston reaches the cylinder head at almost full speed, rebounds slightly from the elastic shock absorber and stops. A long operation in this mode is fraught with a high vibration and may result in a machine damage. A noise emission level becomes uncomfortable.

5 Summary and outlook

The conductance of the end cushioning throttle is usually the once parameter that a user can adjust to reach the desirable damping quality and travel time, when taking a pneumatic drive into operation or maintaining it. The quality of the cushioning process can be quantified using an integral criterion of cushioning time, peak deceleration, and the maximum capability on energy absorption. The damping quality is not equal for the same throttle opening when operating the cylinder drive under various supply pressures, travel speeds and inertial loads. Hence, the global aim of the analysis of integrated pneumatic end cushioning systems is to figure out, how the geometry of the cushioning throttle and cylinder can be designed to guarantee a fast and repeatable deceleration and to minimize the sensitivity against fluctuating operation parameters, such as pressure, moving mass, friction and load forces. This problem can be solved by the multiparametric robust optimization of the end cushioning.

For this purpose, a one-dimensional simulation model of the pneumatic cylinder with an integrated pneumatic cushioning system was developed and is presented in this paper. Different aspects, mainly the parameterization of the friction model and the end cushioning throttle of a real cylinder are discussed in detail. A more accurate alternative to the classical Stribeck-function is proposed to calculate the friction force over a wide range of pressures and speeds.

The simulated piston stroke, pressure and temperature in the end cushioning volume are experimentally validated. The comparison plots, presented in the fig. 10-11, show consistency of the stroke and pressure profiles. In the positive region (above 0 °C) temperatures match good as well. However, the amplitude of simulated temperature in the negative range appears to be higher (up to -20…-30 °C) than it was really measured. That can be caused by a little-known transient behaviour of the temperature sensor under varying flow conditions. Another reason can be a simplification of the cylinder geometry and its thermal model that hides the complex thermal interrelations between the cylinder body and the gas flow. Hence, this approach is a compromise between the high detail degree, which can be enhanced by coupling the present one-dimensional model with a two- or three-dimensional model

solved with finite element and finite volumes methods, and the simulation time. Simulation time is essentially important for sensitivity analysis and robust optimization within the further steps because it may require up to 100,000 number of model runs. Thus, the designed one-dimensional model with simulation time varying between some tenths of the second up to few seconds is considered to be proper for both sensitivity analysis and robust optimization whilst having an acceptable level of representativeness of the real matter.

Funding sources

This research is funded by the European Social Fund and co-financed by tax funds based on the budget approved by the members of the Saxon State Parliament.

Diese Maßnahme wird mit Mitteln aus dem Europäischen Sozialfonds gefördert und mitfinanziert durch Steuermittel auf Grundlage des von den Abgeordneten des Sächsischen Landtags beschlossenen Haushaltes.

Annex

Annex A: Results of a two-dimensional approximation of measured friction force with eq. (4).

related pressure	F_{FC}, N	F_{FS}, N	v_S, m/s	k_v, kg/s	a, -	k_p, N/bar_{rel}	RSS	R^2
p_{AB-}	2 *(constraint)*	12.32	0.001 *(constraint)*	111.5	0.8914	12.56	$4.29 \cdot 10^3$	0.9797
p_{AB+}	2 *(constraint)*	14.45	0.00151	133.5	0.8497	0.994	$5.99 \cdot 10^3$	0.9716

Annex B: Results of a one-dimensional approximation of measured friction force with eq. (7).

p_0, bar_{rel}	b, N	F_{FS}, N	F_{FC}, N	v_S, m/s	k_v, kg/s	a, -	RSS	R^2
2.07	5.447	20.46	5.94	0.00367	102.5	0.6796	9.85	0.9993
3.127	2.824	22.59	5.273	0.004483	106.1	0.7018	9.28	0.9995
4.115	1.468	25.78	6.407	0.004925	123.7	0.6513	17.08	0.9993
5.14	2.776	25.05	4.31	0.004033	128.7	0.6843	7.07	0.9998
6.13	2.509	25.51	3.855	0.003434	140.8	0.662	23.72	0.9993
7.085	1.274	32.95	7.864	0.005579	147.6	0.6468	28.9	0.9992
8.075	-1.17	31.08	5.856	0.005311	158.8	0.6317	26.59	0.9994

Annex C: Results of a two-dimensional approximation of measured friction force with eq. (8) for the main stroke and the end cushioning zone

related pressure	b_0, N	b_1, N/bar_{rel}	$F_{FS.0}$, N	$F_{FS.1}$, N/bar_{rel}	F_{FC}, N	v_S, m/s	$k_{v.0}$, kg/s	$k_{v.1}$, $kg/s/bar_{rel}$	a, -	RSS	R^2
p_{AB-}	-0.67	-4.4	21.64	11.78	5.08	$4.16 \cdot 10^{-3}$	49.9	43.41	0.429	526	0.9974
p_{AB+}	5.63	-0.1	17.06	0.714	5.4	$3.98 \cdot 10^{-3}$	87.46	6.1	0.746	654	0.9969
p_{EC}	9.66	0.26	8.8	2.197	8.8	$2.96 \cdot 10^{-3}$	121	19.61	1	$1.73 \cdot 10^5$	0.9292

Nomenclature

Designation	Denotation	Unit
κ	Isentropic exponent	-
ρ	Density	kg/m^3
a	Speed exponent	-
A	Cross-section area	m^2
b	Friction force bias	N
C	Sonic conductance	$s \cdot m^4/kg$
F	Force	N
h	Specific enthalpy	J/kg

m	Mass	kg
$\dot{m}$	Mass flow rate	kg/s
l	Length	m
k_p	Pressure-dependent friction coefficient	N/bar
k_v	Speed-dependent friction coefficient	kg/s
p	Pressure	bar
$\dot{Q}$	Heat flow	W
t	Time	s
R	Specific gas constant	J/kg/K
T	Temperature	°C, K
$\dot{U}$	Inner energy change	W
v	Speed	m/s
V	Volume	m³
$\dot{W}$	Power	W
x	Coordinate	m
$\dot{x}$	Speed	m/s
$\ddot{x}$	Acceleration	m/s²
z	Number of throttle revolutions	-

Index

Designation	Relation to
1	Inlet conditions
2	Outer conditions
a	Atmospheric conditions acc. to ISO 6358
A	Cylinder chamber A
AB–	(Pressure) difference in A and B
AB+	Sum (of pressures) in A and B
B	Cylinder chamber B
CP	Cushioning plug
EC	End cushioning
FC	Coulomb friction
Fr	Friction
FS	Static friction
L	Load
M	Moving (mass)
MO	Meter-out (throttle)
R	Rod

References

[1] EnEffAH Energy efficiency in production in the drive and handling technology field: Basic principles and measures. EnEffAH Project Consortium, Stuttgart, 2012. Last access on February 12, 2021: https://www.eneffah.de/EnEffAH_Broschuere_engl.pdf.

[2] M Doll. *Optimierungsbasierte Strategien zur Steigerung der Energieeffizienz pneumatischer Antriebe*. Dissertation, Shaker Verlag, Aachen, 2016.

[3] White paper: ACE NoCushion Serie. Externe Endlagendämpfung für Pneumatikzylinder.

[4] White paper: AIRTECs InnoMotix®-System. Pneumatik ohne Dämpfer.

[5] Y T Wang et al. Computer Simulation of a Shock-Absorbing Pneumatic Cylinder. *Journal of Sound and Vibration*, 93(3):353-364, 1984.

[6] P Beater. Endlagendämpfung pneumatischer Zylinder. *O+P Ölhydraulik und Pneumatik*, 47 (2003), No. 3: 163-167, 2003.

[7] X B Tran et al. A new Mathematical Model of Friction for Pneumatic Cylinders. *Proceedings IMechE, Part C: J Mechanical Engineering Science*, Vol. 230(14):2399–2412, 2016.

[8] A C Valdiero et al. Nonlinear Mathematical Modeling in Pneumatic Servo Position Applications. *Hindawi Publishing Corporation: Mathematical Problems in Engineering*, Vol. 2011, Article ID 472903:1-16, 2011. doi:10.1155/2011/472903.

[9] J Hepke. *Energetische Untersuchung und Verbesserung der Antriebs-technik pneumatischer Handhabungssysteme*. Dissertation, Shaker Verlag, Aachen, 2017.

[10] S Klotzbach, H Henrichfreise. Ein nichtlineares Reibmodell für die numerische Simulation reibungsbehafteter mechatronischer Systeme. *Proceeding of 16. Symposium Simulationstechnik in Rostock, 10.-13. September 2002*, pp. 1-13, 2002.

[11] L Endler et al. Compressed air saving in symmetrical and asymmetrical pneumatic positioning systems. *Proceedings IMechE, Part I: J Systems and Control Engineering*, Vol. 229(10):957-969, 2015.

[12] C Jianfeng. Study on Friction Characteristics of Pneumatic Cylinders Base on LuGre Model. *The 6th national fluid drive and control conference proceedings*, 2010:1-5.

[13] Y Zhan et al. Study on Friction Characteristics of Energizing Pneumatic Cylinders. *Advanced Materials Research,* Vol. 904:306-310, 2014. doi:10.4028/www.scientific.net/AMR.904.306.

[14] A Krämer, J Kempkes. Modellierung und Simulation von nichtlinearen Reibungseffekten bei der Lageregelung von Servomotoren, *FHWS Science Journal*, Jg. 1, No. 2:47-57, 2013.

[15] H Watter. *Hydraulik und Pneumatik*. Friedr. Vieweg & Sohn Verlag | GWV Fachverlage GmbH, Wiesbaden, 2007.

[16] T Radermacher et al. *Potenzialstudie Energie-/Kosteneinsparung in der Fluidtechnik.* Final Report. Umweltbundesamt, Reihe Climate Change 19/2021, 2021. Last access on April 30, 2021: https://www.umweltbundesamt.de/sites/default/files/medien/5750/publikationen/2021-04-26_cc_19-2021_fluidtechnik.pdf.

[17] O P Heipl. *Experimentelle und numerische Modellbildung zur Bestimmung der Reibkraft translatorischer Dichtungen*. Dissertation, Shaker Verlag, Aachen, 2013.

[18] G Belforte et al. Measurement of Friction Force in Pneumatic Cylinders. *Tribotest Journal* 10-1, September 2003. (120):33-48, 2003.

[19] A Muth. *Reibkraftermittlung an pneumatischen Ventilen und Zylindern*. Dissertation, Shaker Verlag, Aachen, 1998.

[20] F M White. *Fluid Mechanics*. 8th edition in SI units, McGraw-Hill Education, 2016.

[21] L Pasieka. The applicability of the mass-flow-model according to iso 6358 with the parameter critical conductance c and critical pressure ratio b for gases in high-pressure range up to 300 bar. *Proceeding of 12th International Fluid Power Conference (12. IFK), Dresden*, Vol. 1:541-550, 2020.

[22] H P Bala. Durchflussmessungen und strömungstechnische Kenngrößen. *O+P Ölhydraulik und Pneumatik*, 45 (2001), No. 4:246-255, 2001.

[23] J M Hassan et al. Experimental investigation of a temperature change inside pneumatic cylinder chambers. *Al-Nahrain Journal for Engineering Sciences (NJES)*, Vol. 20 No.1:1-4, 2017.

[24] J F Carneiro, F Gomes de Almeida. Heat transfer evaluation of industrial pneumatic cylinders. *Proceedings IMechE, Part I: J. Systems and Control Engineering,* Vol. 221:119-128, 2007.

[25] R De Giorgi et al. Dynamic thermal model of a discharging process of a pneumatic chamber. *Proceedings of 4th FPNI-PhD Symposium, Sarasota*, pp. 571-583, 2006.

[26] S Michel, J Weber. Prediction of the thermo-energetic behaviour of an electrohydraulic compact drive. *Proceeding of 10th International Fluid Power Conference (10. IFK), Dresden*, pp. 219-233, 2016.